Measuring the Tensile Strain of Wood by Visible and Near-Infrared Spatially Resolved Spectroscopy

---

Te Ma, Tetsuya Inagaki, Masato Yoshida, Mayumi Ichino, and Satoru Tsuchikawa*

***Corresponding author: Satoru Tsuchikawa,** Graduate School of Bioagricultural Sciences, Nagoya University, Furo-Cho, Chikusa, Nagoya 464-8601, Japan, Email addresses: st3842@agr.nagoya-u.ac.jp

Te Ma (mate@agr.nagoya-u.ac.jp), Tetsuya Inagaki (inatetsu@agr.nagoya-u.ac.jp), Masato Yoshida (yoshida@agr.nagoya-u.ac.jp), and Mayumi Ichino (ichino.mayumi@j.mbox.nagoya-u.ac.jp): Graduate School of Bioagricultural Sciences, Nagoya University, Furo-Cho, Chikusa, Nagoya 464-8601, Japan.

Declarations:

Funding: This study is supportted by JSPS (KAKENHI, no.19K15886)

Conflicts of interest/Competing interests: Not applicable

Availability of data and material: Yes

Code availability: Not applicable

Authors' contributions:

Te Ma: methodology, data collection and analysis, writing-original draft preparation

Tetsuya Inagaki: methodology, data validation, and writing- reviewing.

Masato Yoshida: contributed to capture the submicroscopic changes during tension testing, writing- reviewing

Mayumi Ichino: data collection and analysis

Satoru Tsuchikawa*: supervision, conceptualization, writing- reviewing and editing

Ethics approval: Not applicable

Consent to participate: Not applicable

Consent for publication: Not applicable

Abstract:

Strain measurement is critical for wood quality evaluation. Using conventional strain gauges constantly is high cost, also challenging to measure precious wood materials due to the use of strong adhesive. This study demonstrates the correlation between the light scattering degrees inside the wood during tension testing and their macroscopic strain values. A multifiber-based visible-near-infrared (Vis-NIR) spatially resolved spectroscopy (SRS) system was designed to rapidly and conveniently acquire such light

scattering changes. For the preliminary experiment, samples with different thicknesses, from 2 mm to 5 mm, were measured to evaluate the influence of sample thickness. The differences in Vis-NIR SRS spectral data diminished with an increase in sample thickness, suggesting that the SRS method can successfully measure the wood samples' whole strain (i.e., surface and inside). Then, for the primary experiment, 18 wood samples were each prepared with approximately the same sample thickness of 2 mm and 5 mm to construct strain calibration models, respectively. The prediction accuracy of the 2-mm samples was characterized by a determination coefficient (R^2) of 0.81 with a root mean squared error (RMSE) of 343.54 $\mu\varepsilon$ for leave-one-out cross-validation; for test validation, the validation accuracy was characterized by an R^2 of 0.76 and an RMSE of 395.35 $\mu\varepsilon$. For the validation accuracy of the 5-mm samples, R^2_{val} was 0.69 with 440.78 $\mu\varepsilon$ $RMSE_{val.}$ Overall, the presented calibration results of the SRS approach were confirmed to be superior to the standard diffuse reflectance spectroscopy.

Keywords:

Tensile strain of wood; non-destructive evaluation; spatially resolved spectroscopy; visible and short-wave light scattering; multivariate analysis

1. Introduction

Wood is a natural material with multi-layered elongated cells. Due to the variability of its mechanical properties, the tensile strain evaluation of each structural wooden member is critical for quality management (Wang et al. 2020). The strain (ε) is defined as the ratio of the change in length to the original length; it is a unitless quantity (Ambrose 1993). The wood cell wall is a macromolecular composite formed of cellulose, hemicelluloses, and lignin (Hon and Chang 1984). Cellulose is the primary component in bearing tensile stress (Salmén and Bergström 2009). In contrast, hemicelluloses function as a coupling agent to hold the cellulose (Burgert 2006). The conventional method for wood strain measurement is to use a strain gauge, which is high cost (either disposable or reusable ones) in constant use (Yang et al. 2005). In addition, it is challenging to measure precious wood materials due to the use of a strong adhesive, which can destroy the wood after removal. For example, the heritage community generally does not apply strain gauges on genuine objects of art (Anaf et al. 2020). Moreover, difficulties arise when strain gauges are used in an environment where the electromagnetic wave interference is extensive. Such an environment can affect the measurement accuracy or even damage the experimental instruments (Liu et al. 2015; Barr et al. 2017).

In addition to the strain gauge, the wood strain can also be evaluated by monitoring the displacements that occurred during deformation, i.e., digital image correlation (DIC) techniques (Samarasinghe and Kulasiri 2000; Ozyhar et al. 2012). X-ray diffraction (Kamiyama et al. 2005) and infrared (IR) spectroscopy (Åkerholm and Salmén 2001; Salmén and Bergström 2009) can detect wood structure-function relationships at the nano- and microstructural levels. Near-IR (NIR) spectroscopy (wavelength: 800–2500 nm or wavenumber: 12500–4000 cm^{-1}) is another well-suited method in wood research, mainly in combination with multivariate mathematical techniques (Tsuchikawa 2007; Watanabe et al. 2012; Hein et al. 2017). When NIR light illuminates and transmits through an object, the energy of the incident electromagnetic wave changes due to the stretching and bending vibrations of chemical bonds, such as O–H, N–H, and C–H. Subsequently, the quality and quantity of an object can be evaluated non-destructively, rapidly, and cost-effectively by analyzing the light reflectance and transmittance values (Tsuchikawa and Kobori 2015; Ma et al. 2020). Compared with microtomed sections needed for IR spectroscopy, NIR spectroscopy can non-destructively measure wood samples up to several millimeters thick without special sample pretreatments. It is essential when focusing on practical applications, as thin samples prepared in lab behave differently than solid wood, e.g., including stress relaxation in the former (Yu et al. 2009). Taking the

91 advantages of NIR spectroscopy, Guo and Altaner (2018) analyzed band shifts and band
92 assignments on NIR light absorbance characteristics during the wood tension test, the
93 results of which suggest that the observed band shifts correlate with wood tension levels.
94 Their study is impressive and has reference value for future use of NIR spectroscopy (Guo
95 et al. 2019). However, since the molecules are influenced by neighboring molecules,
96 actual peaks generally overlap on the NIR spectra (Okazaki 2012). Although advanced
97 curve-fitting approaches could be used to predict the small-signal peak shift, the band
98 shift may also vary among specimens, which has been confirmed by the IR method
99 (Eichhorn 2001). Additionally, the spectral information of such long-wave sensitive
100 spectrometers is relatively rich, and, as such, it requires expensive equipment, such as
101 detectors and light sources (Xing et al. 2008). Accordingly, there is still room to develop
102 and improve NIR spectra collection and data analysis methods, especially for on-site
103 application purposes.
104
105 The most likely to be neglected is that bulk wood is a highly scattering medium.
106 Studies show that the reduced light scattering coefficient ($\mu_s' = 10 - 100\ cm^{-1}$) is much
107 larger than the absorption coefficient ($\mu_a = 0.05 - 1.00\ cm^{-1}$) in the wavelength range
108 of 700-1040 nm for both softwood and hardwood species treated in different ways (dry,

109 wet and degraded) (D'Andrea et al. 2007). The light scattering degree inside the wood
110 cell wall highly correlates with the microstructure (Ban et al. 2018; Ma et al. 2018a, 2019).
111 The deformation under longitudinal tension includes macromolecule deformations in the
112 layers and interlaminar slippages. The former is related to the structure, orientation, and
113 interaction of the polymers in the wood, and the latter slippage deformation results from
114 the structural differences between cell-wall layers (Keckes et al. 2003; Adler and Buehler
115 2013). For example, the misalignment between the cellulose fibrils to the strain direction
116 could be amplified by bending and shearing (Montero et al. 2012; Salmén 2015).
117 Moreover, the weak interfaces of wood cells or annual rings could deflect transverse
118 cracks into the longitudinal plane (Smith et al. 2003; Marthin and Kristofer Gamstedt
119 2019; Guo et al. 2020). Hence, effective utilization of the light scattering degrees (i.e.,
120 microstructure changes) inside the wood during tension testing should predict strain
121 levels accurately. This method also can reduce costs associated with equipment because
122 shorter wavelengths are scattered more strongly than longer wavelengths in the visible
123 (Vis)–NIR optical range (Ma et al. 2018a).
124
125 Conventional Vis-NIR spectrometry has the potential to gather information on both
126 molecular and anatomical strain. However, since it generally acquires spectral data from

127 a single sample point based on the collective effects of light absorption (due to chemical
128 components such as water and cellulose content) and scattering (due to physical structures
129 such as cell size and intercellular spacing) (Vanoli et al. 2020); studies have mainly relied
130 on performing further spectral pretreatments, such as baseline offset correction or
131 standard normal variate (SNV), to reduce light scattering effects before training
132 calibration models (Zude et al. 2011). By contrast, spatially resolved spectroscopy (SRS)
133 requires relatively strong, steady-state spotlights for illumination; its diffusely reflected
134 light pattern is collected at multiple distances for light absorption and scattering
135 evaluation (Farrell et al. 1992; Qin et al. 2009; Lu et al. 2020). SRS has two main
136 measurement configurations: spectral imaging and fiber probing. On the one hand, the
137 SRS based on spectral imaging is a non-contact method that measures spatially resolved
138 diffuse reflectance over a broad spectral range (Peng and Lu 2008; Qin and Lu 2008; Zhu
139 et al. 2015). The measurement system mainly consists of a hyperspectral imaging (HSI)
140 camera, a prime lens, and a small broadband beam as illumination. However, the distance
141 between the light beam and the source-detector is required to be carefully considered in
142 this configuration, as they determine the measured results (Cen and Lu 2010; Lu et al.
143 2020). On the other hand, the fiber probe-based SRS is a contact method, which is often
144 inconvenient for rapid online quality assessment (Ma et al. 2018a). However, due to the

145 easy-to-operate design with a strong light reflectance, fiber probe-based SRS portable
146 systems are desirable alternatives for on-site applications. Additionally, the contact
147 measurement is more convenient to predict the tension strains of wood samples.

148 This paper reports on wood strain prediction results obtained by evaluating the changes
149 in Vis-NIR SRS spectral data collected from wood samples during tension testing. The
150 objectives of this paper are as follows: (1) acquire light scattering characteristics in wood
151 samples during tension testing by a newly designed multifiber-based Vis-NIR SRS
152 system; (2) examine the relationship between SRS signals and wood strains by principal
153 component analysis (PCA); (3) construct wood strain calibration models by partial least
154 squares (PLS) regression; and (4) benchmark against standard diffuse reflectance
155 spectroscopy to quantify the added value of the SRS method. This study should provide
156 new insights to predict the tensile strain of wood samples conveniently and cost-
157 effectively.

158

159 **2. Materials and methods**

160 **2.1 Sample preparation**

161 Wood samples (*Hinoki cypress*) with a length of 120 mm (longitudinal), a width of
162 10 mm (radial), and various thicknesses (tangential: 2 mm, 3 mm, 4 mm, and 5 mm) were

sawn from air-dried wood board that commercially purchased from a local wood processing company. Specimens were selected from mature wood parts sufficiently far from the pith to neglect ring curvature.

For the preliminary experiment, samples with different thicknesses (2 mm, 3 mm, 4 mm, and 5 mm) were measured to evaluate the influence of sample thickness. Then, for the primary experiment, 18 wood samples were each prepared for approximately the same thickness 2 mm and 5 mm to construct strain calibration models, respectively. The samples were selected based on the wood fiber directions, which were as parallel as possible to the longitudinal direction. Before the experiment, all the pieces remained in a desiccator, where relative humidity (RH) was controlled at 59% with a saturated salt solution of sodium bromide. Subsequently, the sample weights were measured using a digital balance (accuracy of 0.0001 g). A digital caliper (0.01 mm accuracy) was used to measure the sample dimensions. From the measured weights and dimensions of the raw data, sample moisture content (MC) and density were calculated according to the following equations:

$$\mathrm{MC}(\%) = \frac{W - W_d}{W_d} \quad (1)$$

$$\mathrm{Density}\left(\frac{kg}{m^3}\right) = \left(\frac{W}{V}\right) \quad (2)$$

where W is the sample weight before spectral data acquisition and W_d is the sample weight after oven-drying, and V is the sample volume under the equilibrated condition.

2.2 Tensile testing

Each prepared wood sample was placed in a bending testing machine (either Shimadzu AG-100KNI, Shimadzu, Japan or SVZ-50NA, IMADA-SS Corporation, Japan was used depending on the sample thickness and experiment schedule). The bending machine was suspended several times manually during the tension test to obtain strain measurements and Vis-NIR SRS data. The strain was recorded with strain gauges (FLAB-5-11, Tokyo Sokki Kenkyujo, Japan) glued to one side of each sample with instant adhesive (CN, Tokyo Sokki Kenkyujo, Japan) and connected to a strain-meter (TC-32K, Tokyo Sokki Kenkyujo, Japan). A Vis-NIR measurement system was used to collect light scattering characteristics on the other sample side (Fig. 1 (a) and (b)).

2.3 Visible and near-infrared spatially resolved spectroscopy measurements

Fig. 1 (c) and (d) show the measurement part (i.e., the fixator of light illumination and detection fibers) of the proposed Vis-NIR SRS system and a diagram of the internal

198 structure. A 5-W halogen lamp initially provided light illumination. An optical fiber
199 (SOG-70S, Sumita Optical Glass, Inc., Saitama, Japan) translated the light source onto
200 each wood sample. Then, 30 silica fibers (Vis-NIR type, Core: 100 μm, Clad: 110 μm,
201 Fiberguide Industries, New Jersey, USA) were separated into five groups (1, 2, 3, 4, and
202 5 from the light illumination point) to collect the diffusely reflected light and transfer the
203 light to the Vis-NIR HSI camera (SPECT-100nir1F, Spectral Application Research
204 Laboratory Co., Ltd. Shizuoka, JAPAN). A fiber connecter was used to order the 30 silica
205 fibers horizontally at the side of the HSI camera. Then, the light beam was dispersed by
206 a spectrometer into spectral components (vertical axis) while preserving spatial
207 information (horizontal axis), and the two-dimensional light signals were collected. The
208 shutter speed and framerate were set at 15 ms and 8 fps, respectively. In this study, the
209 fixator was pasted parallelly to the sample grain direction with a double-sided tape, which
210 can be easily removable after measurement collection. The sensitive wavelength range of
211 the Vis-NIR HSI camera was 600–1100 nm, with a spectral resolution of 4.5 nm (a
212 minimum reading width of approximately 0.65 nm/pixel). For each measurement, 16
213 spectral images were captured and their averaged values saved. A barium sulfate white
214 plate was used to reflect the transmitted Vis-NIR light through hinoki wood samples.
215 Light reference was measured using a tailor-made integrating sphere, i.e., a plastic ball

(diameter of 6 cm) covered in barium sulfate. Dark values were measured by turning off the light and covering the light-collection fibers. Wavelengths under 660 nm and over 1002 nm were noisy and unreliable. Thus, a wavelength range of 660–1002 nm was selected for further data analysis. The collected spectra were then converted to the reflectance values by Eq. (3):

$$R_\lambda = \frac{S_\lambda - D_\lambda}{B_\lambda - D_\lambda} \quad (3)$$

where λ denotes the wavelength, S and B are the sample and a white reference spectrum, respectively, and D is the dark spectrum.

A digital camera took photos (16 × amplification) of another wood sample (thickness of 2 mm) before and after the tensile test to understand the submicroscopic changes.

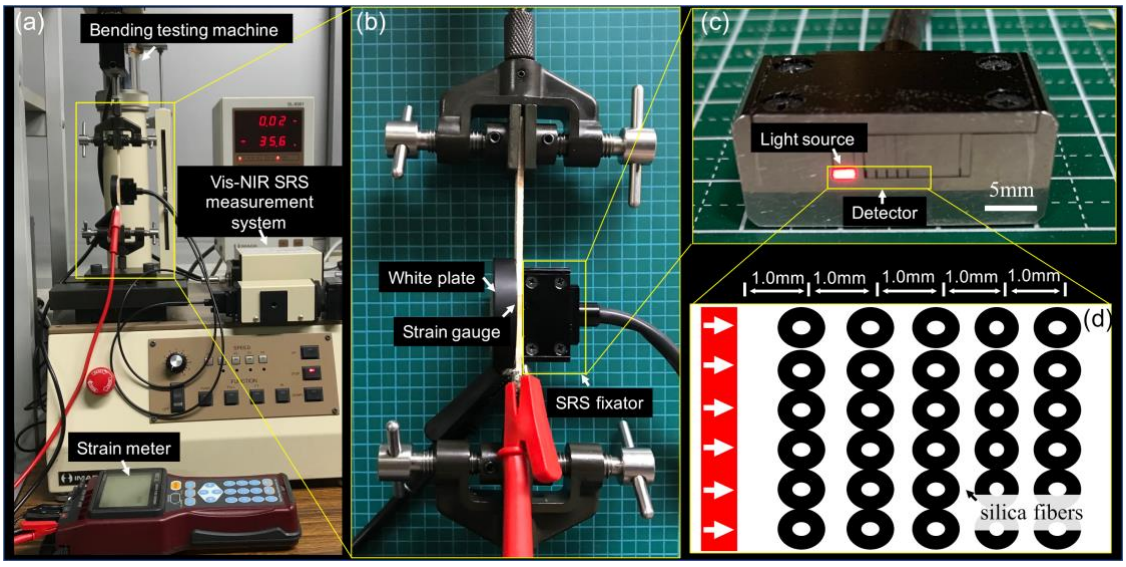

Fig. 1 (a) Experiment instruments; (b) Vis–NIR SRS data and strain measurements; (c) fixator of the Vis-NIR SRS measurement system; (d) internal structure diagram of the fixator.

227 **2.4 Spectra pretreatments and principal component analysis**

228 The Vis-NIR SRS raw spectra were smoothed by a Savitzky–Golay filter (polynomial
229 order: 2; frame length: 15). The spectral data, collected before tension testing subtracted
230 from various strain levels, were tested to correct the natural variability of physical
231 structure among wood samples. Then, PCA with the mean center was used to reduce the
232 dimensionality of the Vis-NIR spectral data while minimizing information loss; the
233 purpose of this was to examine the correlation between measured strain reference values
234 and the spectral data changes. Principal component (PC) loadings are the weights for each
235 variance value of spectral data when calculating the PC scores (Martens and Tormod
236 1992). Generally, the first PC score accounts for the most variability in the original data,
237 and each successive component accounts for as much of the remaining variability as
238 possible (Ma et al. 2020). It is noteworthy that no other spectra pretreatments (e.g., SNV
239 (Cuesta Sánchez et al. 1995) and the second derivative (Gorry 1991)) were used in this
240 study to keep the maximum light scattering information.

241

242 **2.5 Partial least squares regression analysis**

243 To achieve the initial value correction purpose, the Vis-NIR difference spectral data
244 obtained by subtracting the spectrum collected at strain 0 from others were used to

calibrate with the measured strain values via PLS regression (Martens and Tormod 1992). To against overfitting, the wavelength range from 900 nm to 1000 nm was selected from each fiber group (FG). In addition, 70 % of measured data was randomly selected as the calibration set, leaving 30 % for the test set in developing the PLS regression models. Leave-one-out cross-validation was used to optimize the number of latent variables (LVs). The coefficients of determination (R^2) and the root mean squared error (RMSE) characterized the constructed calibration model's performance:

$$R^2 = 1 - \frac{\sum_{i=1}^{n}(y_i - \hat{y}_i)^2}{\sum_{i=1}^{n}(y_i - \bar{y})^2} \quad (4)$$

$$\mathrm{RMSE} = \sqrt{\frac{1}{n}\sum_{i=1}^{n}(\hat{y}_i - y_i)^2} \quad (5)$$

where n is the number of measurements, y is the reference strain values, $\hat{y}$ is the strain value predicted by PLS regression analysis, and $\bar{y}$ is the mean value of y. To quantify the added value of the SRS approach, the PLS calibration results earned by using the total five FGs were also benchmarked against either using the first three FGs or the standard spectroscopy analysis that only using one FG. Data analysis was performed by MATLAB (The MathWorks Inc., Natick, MA).

3 Results and discussion

Fig. 2 shows the raw spectral image of 2-mm wood sample taken by the Vis-NIR HSI camera before the tensile test. This image data contains the spatial information of the 30 silica fibers (horizontal axis) and the spectral information of the measured wood sample (vertical axis). The main difficulty with conventional SRS methods is associated with quickly collecting the spectral data with a high signal-to-noise ratio. One way is to repeat the same data measurements and to average the results, which is time-consuming (Tkachenko 2006). This study is desirable for the spectral data acquisition time to be short of excluding other relaxation phenomena (Burgert 2006; Altaner et al. 2014). This was achieved by a two-step signal averaging process: (i) each fiber occupies 34 pixels of the HSI camera, and the central 30 pixels were averaged for spectral data collection, after which, (ii) the signals of six fibers in the same group were averaged.

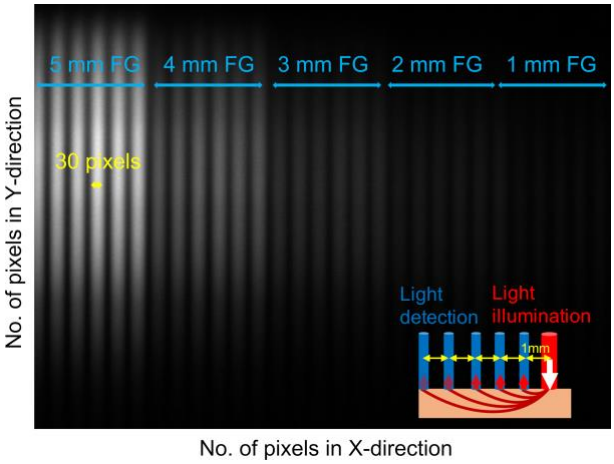

Fig. 2. Raw Vis-NIR SRS spectral image of a wood sample with 2 mm thickness.

Fig. 3 shows the Vis-NIR SRS spectra with standard deviations of the 18 wood samples with approximately the same 2 mm and at various tension levels. It is logical that the overall spectral intensity quickly falls with an increase in distance from the light illumination. The wavelength at 925 nm corresponds to the third overtone of C–H absorption (Mohammadi-Moghaddam et al. 2018), which can be attributed to the chemical components of the wood samples. The wavelength at approximately 930 nm has the highest light reflectance when the FG is 3–4 mm away from the light illumination, suggesting that the light at said wavelength was less absorbed and transmitted further from the light illumination than other wavelengths along the wood grain direction. It is noteworthy that the optical scattering was not isotropic within each wood sample. The light propagated further in the parallel direction because the scattering coefficient along the cylinders is much smaller than that in the perpendicular direction to the grain direction (Ma et al. 2018b, 2019).

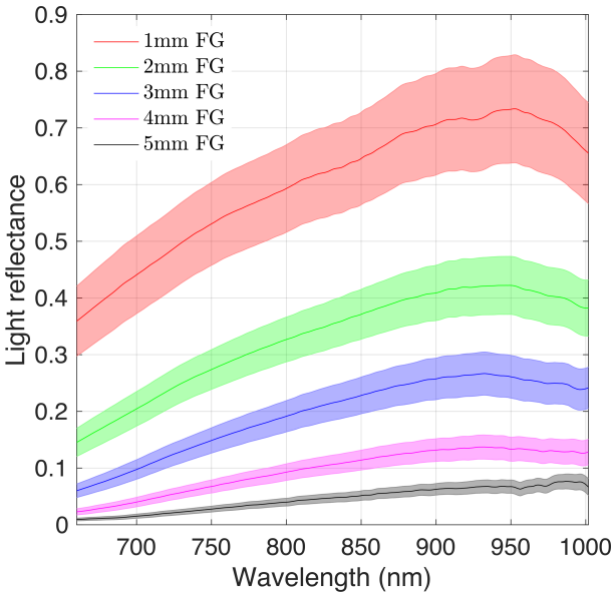

Fig. 3 Averaged Vis-NIR raw spectra and the standard deviations (light color) of 18 samples with the same thickness (2 mm) and various tension strains.

Fig. 4 shows the Vis-NIR spectral data for various strain measurements for wood samples with different thicknesses (vertical) by different FGs (horizontal), respectively. The wavelength range was selected to 900–950 nm to expand the image size. In this study, the Vis-NIR light could transmit through the hinoki wood samples with an maximum thickness of approximately 5 mm (see supplementary, Fig. S1). The light reflectance increased with an increase in wood strain. Light absorption at 925 nm is the most obvious at the spectra collected by the 1-mm FG. The signal quality decreases with an increase in distance between the light illumination and light-detection fibers, suggesting that different FGs can collect spectral data with different light absorption and scattering

296 degrees. Light reflectance is also affected by sample thickness. The differences in the Vis-
297 NIR spectral data, caused by sample strains, diminished in thicker samples, especially at
298 far FGs. This could be due to the light transmission depth is different among the wood
299 samples at various thicknesses. Since thicker wood samples have a more profound light
300 transmission, which affected light propagates in parallel; stronger noise was associated
301 with the collected spectra at more extended FGs. Except for signal quality, because the
302 strain gauge was stuck on the opposite side of the SRS fixator, less transmission light
303 could also reduce the correlation between SRS data and strain reference values. Further
304 improvements could be considered to construct strain prediction models for thicker
305 samples, such as reducing the distance between FGs and introducing a method to measure
306 the strain changes where the spectral data were collected.

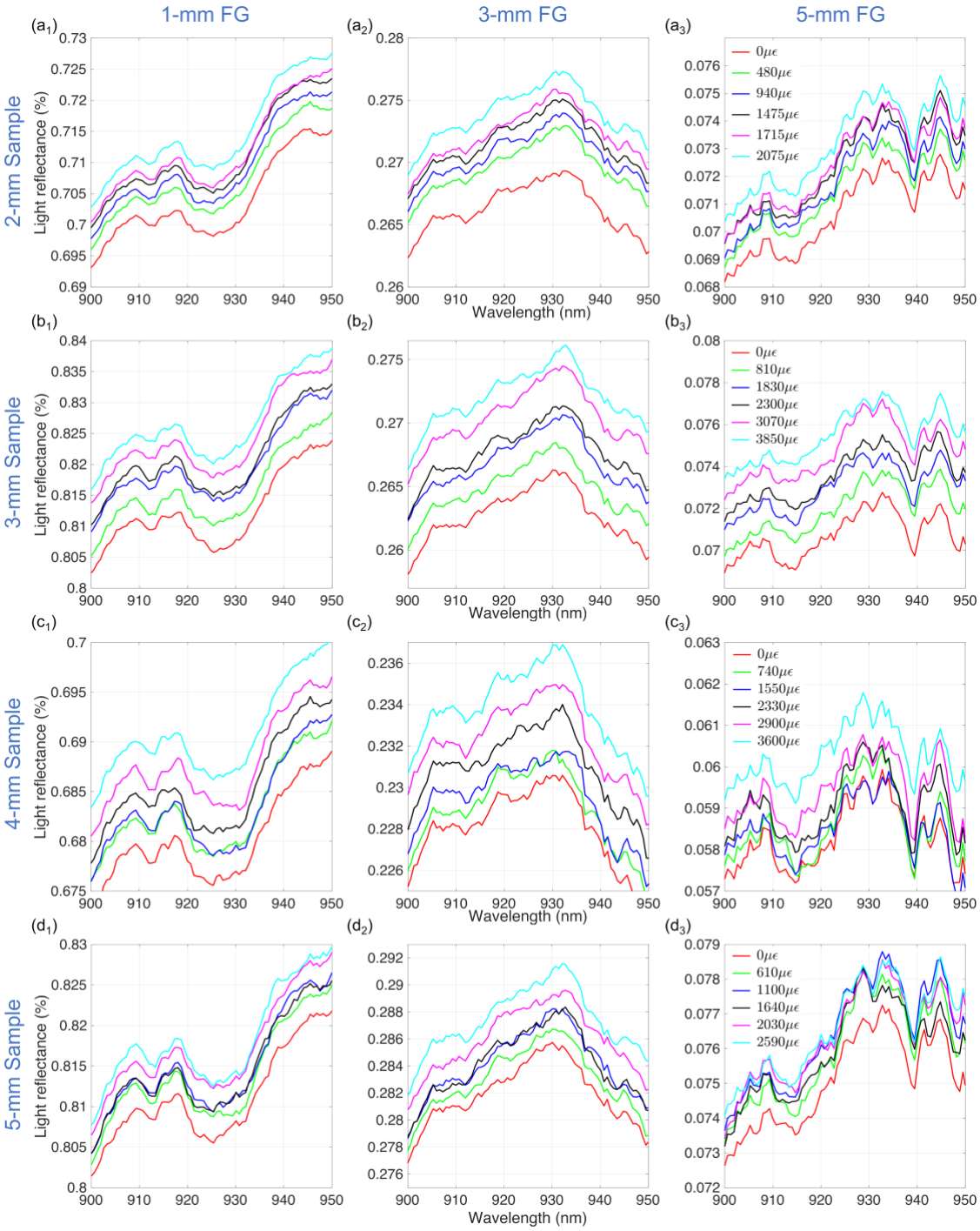

Fig. 4 Vis-NIR SRS spectral data collected at various sample thicknesses (vertical) by different FGs (horizontal).

307

Fig. 5 (b) and (c) show the digital photos of wood samples before and after tension testing with a strain of 3410 με. The stretched wood cell wall could decrease the amount of material in the measured area and increase the light transmissivity on the cell wall between the light source and the five FGs of the SRS fixator. Hence, the light reflectance values increased during the tension test.

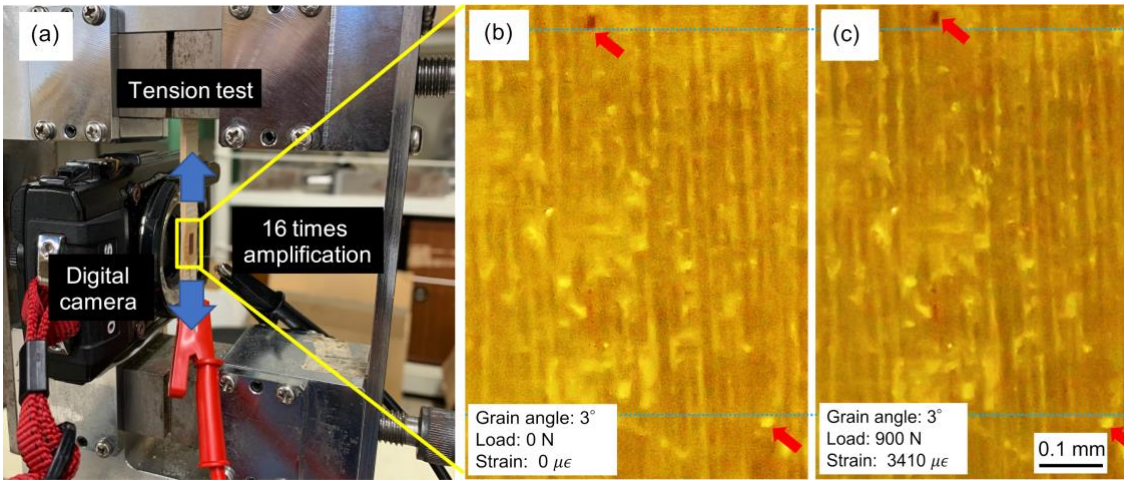

Fig. 5 Digital photos of the wood sample with 2 mm thickness before (a) and after (b) the tension test, respectively.

To check the correlation between measured strain reference values and the spectral data changes. The SRS data collected from the total five FGs at a wavelength range of 660–1002 nm were concatenated, resulting in 2555 variance values (Figure 6 (a_1: 2-mm sample, b_1:3-mm sample, c_1: 4-mm sample, and d_1: 5-mm sample)). Fig. 6 (a_2-d_2)) shows their first two PC loadings. The PC loadings can be understood as the weights for each variance value when calculating the PC score. The accumulated contribution rate of the

320 frist two scores is approximately 99.64%, 99.15%, 97.47%, and 94.48% for a sample
321 thickness of 2, 3, 4, and 5 mm, respectively. The PC1 and PC2 scores of the SRS are
322 shown in Fig. 6 (a_3-d_3), where the Y-axis shows the PC2 score and the X-axis shows the
323 PC1 score. There is a strong correlation between PC1 loading and light scattering
324 differences, i.e., vertical baseline shift. As expected from Fig. 4 (i.e., the differences in
325 the Vis-NIR spectral data diminished in thicker samples), the contribution rate of the PC
326 1 score decreases with an increase in sample thickness. Moreover, PC2 loading has
327 relatively high absolute values at light wavelengths close to water specific band at 970
328 nm. It suggests a meaningful correlation between the light absorption by hydrogen bonds
329 and wood strain changings, but the contribution rate was much lower than the light
330 scattering differences. It could be supported by the knowledge that wood becomes more
331 ductile with increased MC (Ozyhar et al. 2012; Mvondo et al. 2017), which also affects
332 the light scattering degree (Konagaya et al. 2016). This also suggests that MC effects
333 much be fully valued, to build individual calibration models depends on sample MC may
334 be the best way to reduce the MC effects.
335

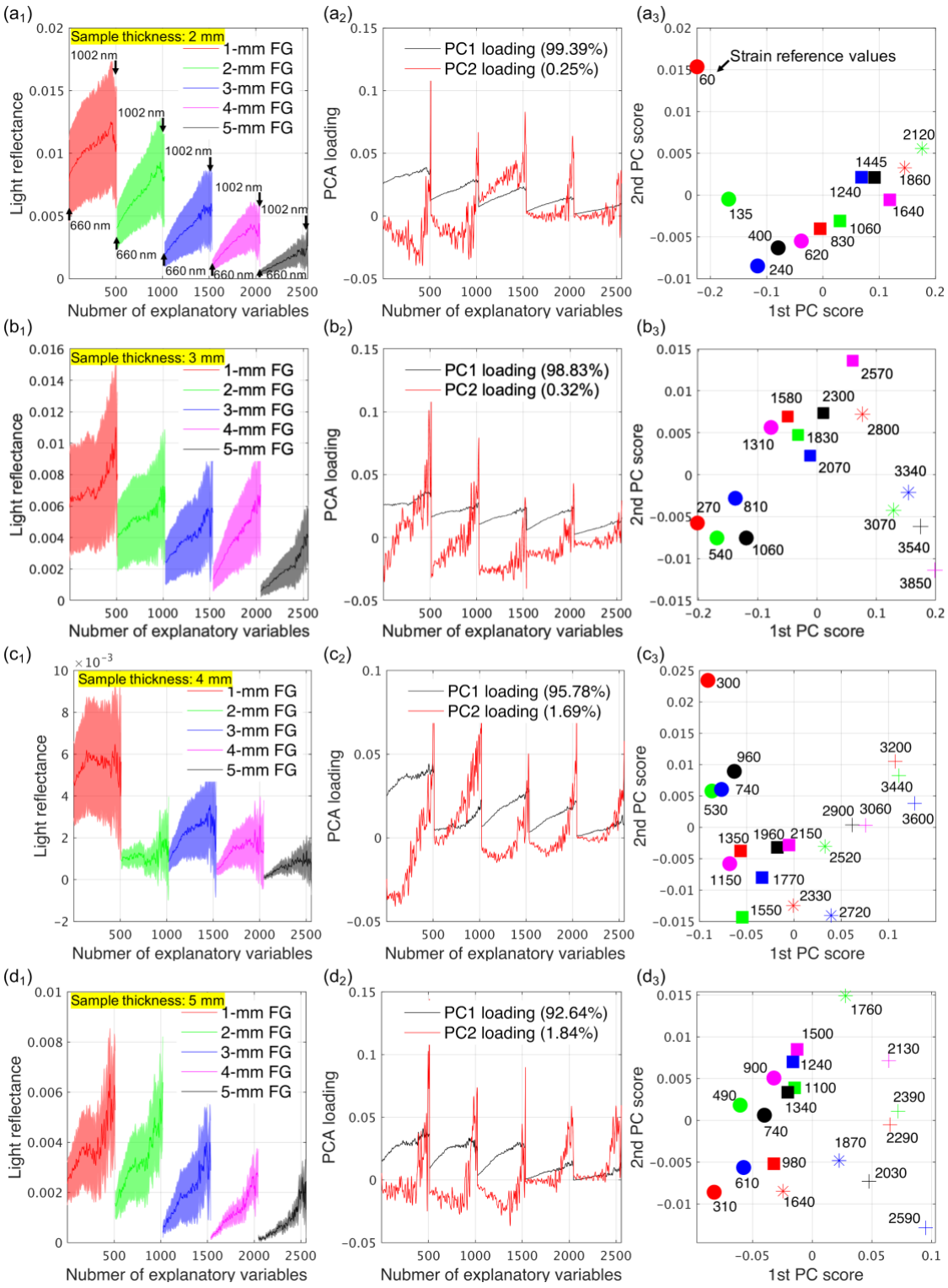

Fig. 6 (a_1-d_1) Concatenated Vis-NIR difference spectral data used for PCA; (a_2-d_2) first two PC loadings; (a_3-d_3) first two PC socres of the concatenated Vis-NIR spectral data. The numbers in each scatter plot show the tensile strain reference values.

Fig. 7 (a_1) shows the strain calibration results of the 18 wood samples with approximately the same thickness of 2 mm from the PLS regression method with the five FGs. The wavelength range of 900-1000 nm was selected from each FG. Fig. 7 (a_{2-3}) shows the RMSE and the PLS regression coefficients regarding the Vis-NIR difference spectra with LV numbers 8, respectively. Table 1 shows the detailed density and MC values of all the wood samples. Overall, the PLS calibration model has a high prediction accuracy: the R^2 and RMSE of the calibration set were 0.81 and 343.54 $\mu\varepsilon$, respectively. For the validation set, the R^2 and RMSE were 0.76 and 395.35 $\mu\varepsilon$, respectively. Differences in the RMSE could be attributed to the strain gauge measured the strain reference values from the wood surface. By contrast, the SRS method measured the light scattering degrees mainly affected by the sample inside structures. Hence, there is a possibility that the SRS method could estimate the wood sample strain more accurately than the conventional strain gauges, but further studies are required to prove this. Fig. 7 (b_{1-3}) shows the calibration results of the same wood samples with the first three FGs (i.e., 1-mm FG, 2-mm FG, and 3-mm FG) and LV numbers 7. Fig. 7 (c_{1-3}) shows the calibration results of the same wood samples with only the first FG (i.e., 1-mm FG) and LV numbers 5. It is evident that the prediction accuracy was improved by increasing the

353 number of FGs, suggesting the effectiveness of the SRS method compared to the

354 conventional NIR spectrometry.

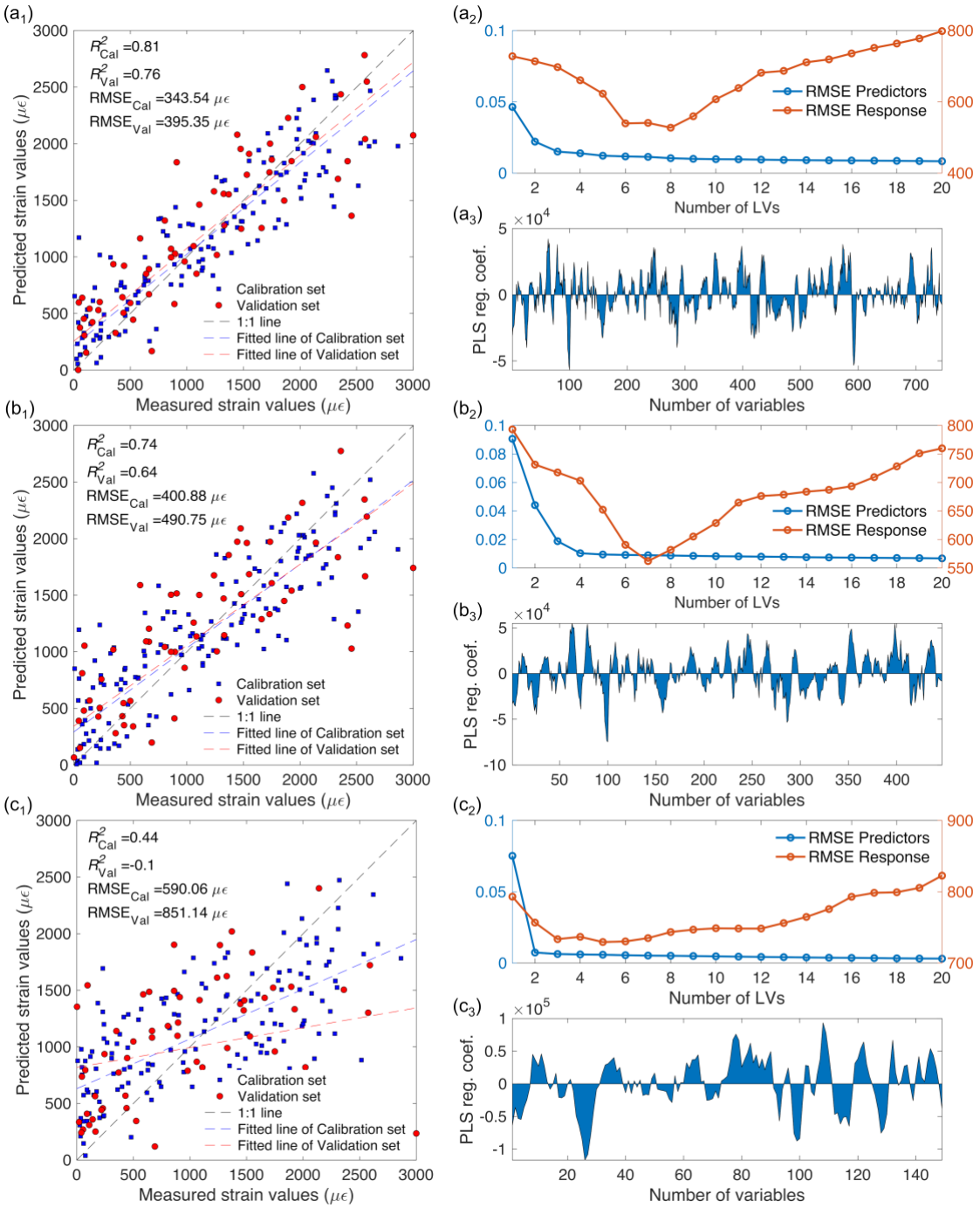

Fig. 7 (a_1-c_1) Scatter plot of measured and predicted strain values of 2-mm wood samples using; (a_2-c_2) RMSE of the predictors and response; (a_3-c_3) PLS regression coefficients.

Fig. 8 ($a_{1\text{-}3}$) shows the strain calibration results of the 18 wood samples with 5 mm thickness from the PLS regression method with the five FGs and LV numbers 7. The same wavelength range of 900-1000 nm was selected from each FG. Table 1 shows the detailed density and MC values of all the samples. Overall, the PLS calibration model had a good prediction accuracy: the R^2 and RMSE of the calibration set were 0.8 and 348.81 $\mu\varepsilon$, respectively. For the validation set, the R^2 and RMSE were 0.69 and 440.78 $\mu\varepsilon$, respectively. Fig. 8 ($b_{1\text{-}3}$) shows the calibration results of the same wood samples with the first three FGs and LV numbers 4. Fig. 8 ($c_{1\text{-}3}$) shows the calibration results of the same wood samples with only the first FG and LV numbers 2. Overall, the strain prediction accuracy of the 5-mm samples was lower than that of the 2-mm wood samples, which agrees that the differences in the Vis-NIR spectral data, caused by sample strains, diminished in thicker pieces. Nevertheless, that does not mean the SRS method can not be used to assess thicker structural timbers. The maximum measurable depth of the hinoki wood samples was confirmed to be approximately 5 mm using the designed Vis-NIR SRS system (see supplementary, Fig. S1); Hence, for thick timbers, the stain prediction would be achieved by estimating the light scattering changes in the sample subsurface layers.

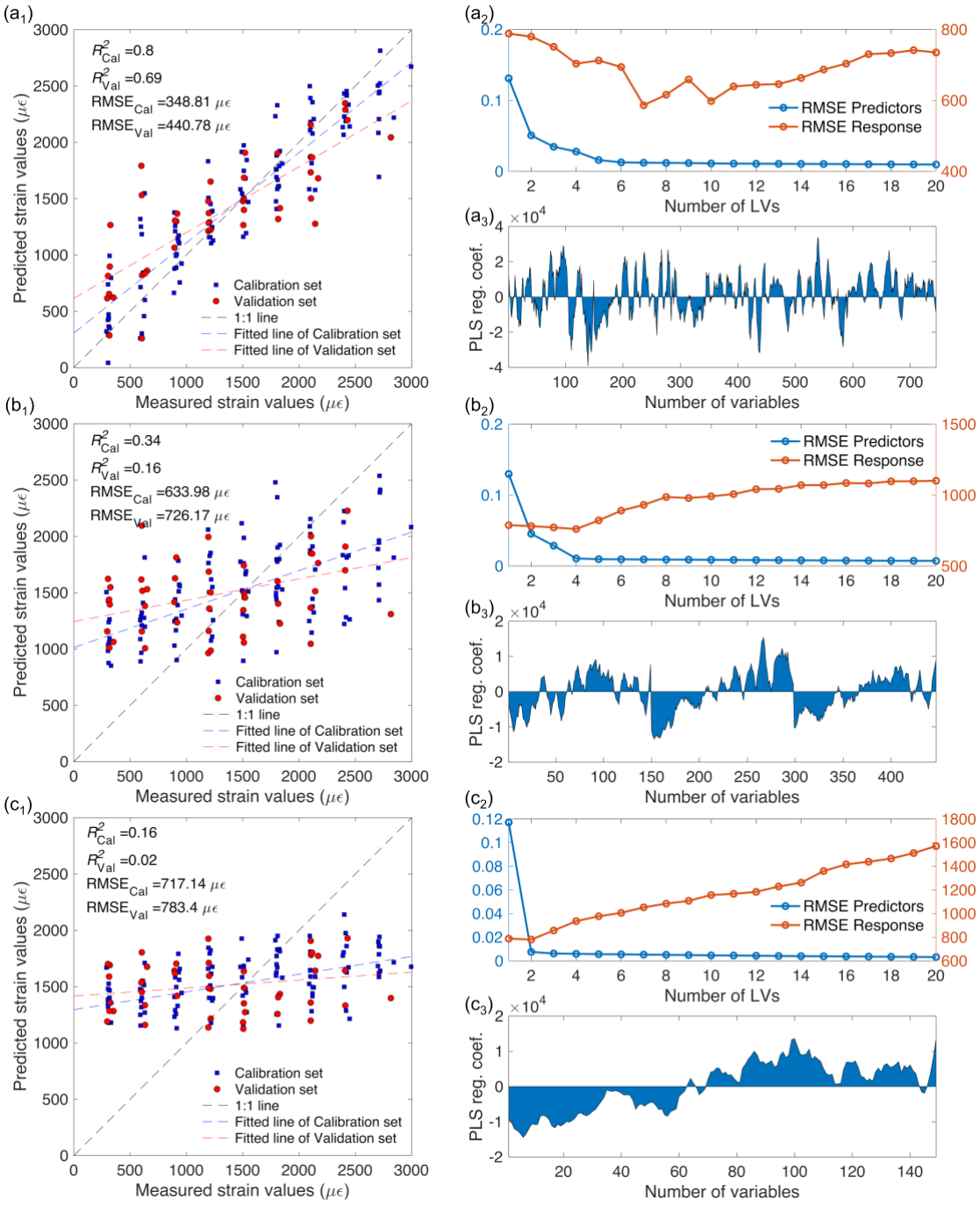

Fig. 8 (a_1-c_1) Scatter plot of measured and predicted strain values of 5-mm wood samples using; (a_2-c_2) RMSE of the predictors and response; (a_3-c_3) PLS regression coefficients.

371

372

373

374

375 Table 1 sample thickness, density, and MC

	2-mm wood samples			5-mm wood samples		
Sample number	Thickness (mm)	Density (kg/m^3)	MC (%)	Thickness (mm)	Density (kg/m^3)	MC (%)
1	2.0	407	11	4.8	369	8
2	2.0	408	11	4.9	421	9
3	1.9	397	11	4.9	435	9
4	1.9	429	10	5.0	443	8
5	1.8	399	10	4.8	421	8
6	1.8	420	10	4.8	438	9
7	1.8	419	11	4.8	473	9
8	1.9	409	10	4.9	451	9
9	2.0	420	10	5.2	435	9
10	2.0	427	11	5.1	462	9
11	2.0	403	11	5.1	430	8
12	2.2	390	11	5.5	408	8
13	2.1	425	10	5.0	435	9
14	2.0	406	10	5.3	442	8
15	2.0	407	10	5.1	439	9
16	2.0	446	10	5.0	393	8
17	2.1	418	10	5.0	379	9
18	1.9	439	10	5.0	461	8

376

377 **4 Conclusion**

378 This study aims to demonstrate the correlation between light scattering changes inside
379 the wood samples during tension testing and their macroscopic strain values. Spatially
380 resolved diffuse reflectance was collected by designing a portable and cost-effective
381 measurement system based on fiber probes. For the preliminary experiment, samples with
382 different thicknesses (2 mm, 3 mm, 4 mm, and 5 mm) were measured to evaluate the
383 influence of sample thickness. Then, for the primary experiment, each 18 wood samples
384 with the same thickness of 2 mm and 5 mm were tested to construct a strain calibration
385 model. The prediction accuracy for the 2 mm samples was characterized by an R^2 of 0.81
386 and an RMSE for 343.54 με for leave-one-out cross-validation, 0.76 and 395.35 μ for test

validation. The R^2 and RMSE of the calibration set for the 5-mm samples were 0.8 and 348.81 με, respectively. For the validation set, the R^2 and RMSE were 0.69 and 440.78 με, respectively.

The designed SRS measurement system does not require sophisticated measurement techniques. Moreover, it has a cost-effective design due to the Vis-NIR HSI camera with short-wave sensitivity, which is much cheaper than long-wave sensitivity cameras. Further research should focus on extending the applicability of the SRS approach to a broader database of wood types and larger sample numbers with various thicknesses. The intervals between FGs should be changed to test the strain prediction of thicker wood samples. This research also references further research to measure growth strain in trees non-destructively. However, because light scattering degree is also affected by MC, this would require more in-depth spectral pretreatments.

5 Acknowledgments

The authors are grateful for the financial support provided by JSPS (KAKENHI, no.19K15886)

6 References

404 Adler DC, Buehler MJ (2013) Mesoscale mechanics of wood cell walls under axial
405 strain. Soft Matter 9:7138–7144. https://doi.org/10.1039/c3sm50183c
406 Åkerholm M, Salmén L (2001) Interactions between wood polymers studied by
407 dynamic FT-IR spectroscopy. Polymer (Guildf) 42:963–969.
408 https://doi.org/10.1016/S0032-3861(00)00434-1
409 Altaner CM, Thomas LH, Fernandes AN, Jarvis MC (2014) How cellulose stretches:
410 Synergism between covalent and hydrogen bonding. Biomacromolecules 15:791–
411 798. https://doi.org/10.1021/bm401616n
412 Ambrose J (1993) Building structures. John Wiley & Sons
413 Anaf W, Cabal A, Robbe M, Schalm O (2020) Real-time wood behavior: The use of
414 strain gauges for preventive conservation applications. Sensors (Switzerland) 20:.
415 https://doi.org/10.3390/s20010305
416 Ban M, Inagaki T, Ma T, Tsuchikawa S (2018) Effect of cellular structure on the optical
417 properties of wood. J Near Infrared Spectrosc 26:53–60.
418 https://doi.org/10.1177/0967033518757233
419 Barr AD, Clarke SD, Tyas A, Warren JA (2017) Electromagnetic Interference in
420 Measurements of Radial Stress During Split Hopkinson Pressure Bar Experiments.
421 Exp Mech 57:813–817. https://doi.org/10.1007/s11340-017-0280-4

422 Burgert I (2006) Exploring the Micromechanical Design of Plant Cell Walls. Am J Bot
423 93:1391–1401
424 Cen H, Lu R (2010) Optimization of the hyperspectral imaging-based spatially-resolved
425 system for measuring the optical properties of biological materials. Opt Express
426 18:17412. https://doi.org/10.1364/oe.18.017412
427 Cuesta Sánchez F, Toft J, van den Bogaert B, et al (1995) Monitoring powder blending
428 by NIR spectroscopy. Fresenius J Anal Chem 352:771–778.
429 https://doi.org/10.1007/BF00323062
430 D'Andrea C, Farina A, Comelli D, et al (2007) Time-resolved diffuse optical
431 spectroscopy of wood. Opt InfoBase Conf Pap 62:569–574.
432 https://doi.org/10.1117/12.727955
433 Eichhorn YRJ (2001) The young's modulus of a microcrystalline cellulose. Cellulose
434 8:197–207. https://doi.org/10.1023/A:1013181804540
435 Farrell TJ, Patterson MS, Brain W (1992) A diffusion theory model of spatially
436 resolved, steady-state diffuse reflectance for the noninvasive determination of
437 tissue optical properties in vivo. Medphys 19:879–888.
438 https://doi.org/10.1118/1.596777

Gorry PA (1991) General Least-Squares Smoothing and Differentiation of Nonuniformly Spaced Data by the Convolution Method. Anal Chem 63:534–536. https://doi.org/10.1021/ac00005a031

Guo F, Altaner CM (2018) Molecular deformation of wood and cellulose studied by near infrared spectroscopy. Carbohydr Polym 197:1–8. https://doi.org/10.1016/j.carbpol.2018.05.064

Guo F, Altaner CM, Jarvis MC (2020) Thickness-dependent stiffness of wood: Potential mechanisms and implications. Holzforschung 74:1079–1087. https://doi.org/10.1515/hf-2019-0311

Guo F, Cramer M, Altaner CM (2019) Evaluation of near infrared spectroscopy to non-destructively measure growth strain in trees. Cellulose 26:7663–7673. https://doi.org/10.1007/s10570-019-02627-2

Hein PRG, Pakkanen HK, Dos Santos AA (2017) Challenges in the use of near infrared spectroscopy for improving wood quality: A review. For Syst 26:1–10. https://doi.org/10.5424/fs/2017263-11892

Hon DNS, Chang ST (1984) Surface Degradation of Wood By Ultraviolet Light. J Polym Sci A1 22:2227–2241. https://doi.org/10.1002/pol.1984.170220923

456 Kamiyama T, Suzuki H, Sugiyama J (2005) Studies of the structural change during
457 deformation in Cryptomeria japonica by time-resolved synchrotron small-angle X-
458 ray scattering. J Struct Biol 151:1–11. https://doi.org/10.1016/j.jsb.2005.04.007
459 Keckes J, Burgert I, Frühmann K, et al (2003) Cell-wall recovery after irreversible
460 deformation of wood. Nat Mater 2:810–814. https://doi.org/10.1038/nmat1019
461 Konagaya K, Inagaki T, Kitamura R, Tsuchikawa S (2016) Optical properties of drying
462 wood studied by time-resolved near-infrared spectroscopy. Opt Express 24:9561.
463 https://doi.org/10.1364/OE.24.009561
464 Liu Q, Ding W, Zhou H, et al (2015) A Novel Strain Measurement System in Strong
465 Electromagnetic Field. IEEE Trans Plasma Sci 43:3562–3567.
466 https://doi.org/10.1109/TPS.2015.2418276
467 Lu R, Van Beers R, Saeys W, et al (2020) Measurement of optical properties of fruits
468 and vegetables: A review. Postharvest Biol Technol 159:111003.
469 https://doi.org/10.1016/j.postharvbio.2019.111003
470 Ma T, Inagaki T, Tsuchikawa S (2019) Three-dimensional grain angle measurement of
471 softwood (Hinoki cypress) using near infrared spatially and spectrally resolved
472 imaging (NIR-SSRI). Holzforschung 73:817–826. https://doi.org/10.1515/hf-2018-
473 0273

474 Ma T, Schajer G, Inagaki T, et al (2018a) Optical characteristics of Douglas fir at
475 various densities, grain directions and thicknesses investigated by near-infrared
476 spatially resolved spectroscopy (NIR-SRS). Holzforschung 1–8.
477 https://doi.org/10.1515/hf-2017-0213
478 Ma T, Schajer G, Inagaki T, et al (2018b) Optical characteristics of Douglas fir at
479 various densities, grain directions and thicknesses investigated by near-infrared
480 spatially resolved spectroscopy (NIR-SRS). Holzforschung 72:789–796.
481 https://doi.org/10.1515/hf-2017-0213
482 Ma T, Tsuchikawa S, Inagaki T (2020) Rapid and non-destructive seed viability
483 prediction using near-infrared hyperspectral imaging coupled with a deep learning
484 approach. Comput Electron Agric 177:.
485 https://doi.org/10.1016/j.compag.2020.105683
486 Martens H, Tormod N (1992) Multivariate calibration. John Wiley & Sons.
487 Marthin O, Kristofer Gamstedt E (2019) Damage shielding mechanisms in hierarchical
488 composites in nature with potential for design of tougher structural materials. R
489 Soc Open Sci 6:. https://doi.org/10.1098/rsos.181733
490 Mohammadi-Moghaddam T, Razavi SMA, Sazgarnia A, Taghizadeh M (2018)
491 Predicting the moisture content and textural characteristics of roasted pistachio

kernels using Vis/NIR reflectance spectroscopy and PLSR analysis. J Food Meas Charact 12:346–355. https://doi.org/10.1007/s11694-017-9646-7

Montero C, Clair B, Alméras T, et al (2012) Relationship between wood elastic strain under bending and cellulose crystal strain. Compos Sci Technol 72:175–181. https://doi.org/10.1016/j.compscitech.2011.10.014

Mvondo RRN, Meukam P, Jeong J, et al (2017) Influence of water content on the mechanical and chemical properties of tropical wood species. Results Phys 7:2096–2103. https://doi.org/10.1016/j.rinp.2017.06.025

Okazaki Y (2012) Near-Infrared Spectroscopy—Its Versatility in Analytical. Anal Chem 28:545–562

Ozyhar T, Hering S, Niemz P (2012) Moisture-dependent elastic and strength anisotropy of European beech wood in tension. J Mater Sci 47:6141–6150. https://doi.org/10.1007/s10853-012-6534-8

Peng Y, Lu R (2008) Analysis of spatially resolved hyperspectral scattering images for assessing apple fruit firmness and soluble solids content. Postharvest Biol Technol 48:52–62. https://doi.org/10.1016/j.postharvbio.2007.09.019

508 Qin J, Lu R (2008) Measurement of the optical properties of fruits and vegetables using
509 spatially resolved hyperspectral diffuse reflectance imaging technique. Postharvest
510 Biol Technol 49:355–365. https://doi.org/10.1016/j.postharvbio.2008.03.010
511 Qin J, Lu R, Peng Y (2009) Prediction of apple internal quality using spectral
512 absorption and scattering properties. Trans ASABE 52:486–499.
513 https://doi.org/10.13031/2013.26807
514 Salmén L (2015) Wood morphology and properties from molecular perspectives. Ann
515 For Sci 72:679–684. https://doi.org/10.1007/s13595-014-0403-3
516 Salmén L, Bergström E (2009) Cellulose structural arrangement in relation to spectral
517 changes in tensile loading FTIR. Cellulose 16:975–982.
518 https://doi.org/10.1007/s10570-009-9331-z
519 Samarasinghe S, Kulasiri G (2000) Displacement fields of wood in tension based on
520 image processing Part 1. Silva Fenn 34:251–259
521 Smith I, Landis E, Gong M (2003) Fracture and fatigue in wood. John Wiley & Sons
522 Tkachenko N V (2006) Chapter 7 - Flash–photolysis. In: Optical Spectroscopy. Elsevier
523 Science, Amsterdam, pp 129–149
524 Tsuchikawa S (2007) A Review of Recent Near Infrared Research for Wood and Paper.
525 Appl Spectrosc Rev 42:43–71. https://doi.org/10.1080/05704920601036707

526 Tsuchikawa S, Kobori H (2015) A review of recent application of near infrared
527 spectroscopy to wood science and technology. J Wood Sci 61:213–220.
528 https://doi.org/10.1007/s10086-015-1467-x
529 Vanoli M, Van Beers R, Sadar N, et al (2020) Time- and spatially-resolved
530 spectroscopy to determine the bulk optical properties of 'Braeburn' apples after
531 ripening in shelf life. Postharvest Biol Technol 168:.
532 https://doi.org/10.1016/j.postharvbio.2020.111233
533 Wang D, Lin L, Fu F (2020) Deformation mechanisms of wood cell walls under tensile
534 loading: a comparative study of compression wood (CW) and normal wood (NW).
535 Cellulose 27:4161–4172. https://doi.org/10.1007/s10570-020-03095-9
536 Watanabe K, Yamashita K, Noshiro S (2012) Non-destructive evaluation of surface
537 longitudinal growth strain on Sugi (Cryptomeria japonica) green logs using near-
538 infrared spectroscopy. J Wood Sci 58:267–272. https://doi.org/10.1007/s10086-
539 011-1238-2
540 Xing Z, Wang J, Shen G (2008) Short-Wave Near-Infrared Spectroscopy for Rapid
541 Quantification of Acidity of Aviation Kerosene. Open Fuels Energy Sci J 1:51–53.
542 https://doi.org/10.2174/1876973x00801010051

543 Yang JL, Baillères H, Okuyama T, et al (2005) Measurement methods for longitudinal
544 surface strain in trees: A review. Aust For 68:34–43.
545 https://doi.org/10.1080/00049158.2005.10676224
546 Yu Y, Jiang Z, Tian G (2009) Size effect on longitudinal MOE of microtomed wood
547 sections and relevant theoretical explanation. For Stud China 11:243.
548 https://doi.org/10.1007/s11632-009-0040-3
549 Zhu Q, He C, Lu R, et al (2015) Ripeness evaluation of “Sun Bright” tomato using
550 optical absorption and scattering properties. Postharvest Biol Technol 103:27–34.
551 https://doi.org/10.1016/j.postharvbio.2015.02.007
552 Zude M, Pflanz M, Spinelli L, et al (2011) Non-destructive analysis of anthocyanins in
553 cherries by means of Lambert-Beer and multivariate regression based on
554 spectroscopy and scatter correction using time-resolved analysis. J Food Eng
555 103:68–75. https://doi.org/10.1016/j.jfoodeng.2010.09.021
556